View metadata, citation and similar papers at core.ac.uk
brought to you by CORE
provided by Aston Publications Explorer

Particle separation by horizontal deflection in paramagnetic fluid

S. Liu[1]*, M. Leaper[2], N.J. Miles[3]

1. Process and Environmental Research Division, Faculty of Engineering, University of Nottingham, University Park, Nottingham, NG7 2RD, United Kingdom

2. Chemical Engineering and Applied Chemistry, Aston University, Birmingham B4 7ET

3. Faculty of Science and Engineering, University of Nottingham Ningbo China, Taikang East Road, Ningbo, 315100, China

Abstract

This paper describes the horizontal deflection behaviour of the streams of particles in paramagnetic fluids under a high-gradient superconducting magnetic field, which is the continued work on the exploration of particles magneto-Archimedes levitation. Based on the previous work on the horizontal deflection of a single particle, a glass box and collector had been designed to observe the movement of particles group in paramagnetic fluids. To get the exact separation efficiency, the method of “sink-float” involved the high density fluid polytungstate (Dense medium separation) and MLA (Mineral Liberation Analyser) were performed. It was found that the particles were deflected and settled at a certain positions on the container floor due to the combined forces of gravity and magneto-Archimedes forces as well as a lateral buoyancy (displacement) force. Mineral particles with different densities and susceptibilities could be deflected to different positions, thus producing groups of similar types of particles. The work described here, although in its infancy, could form the basis of new approach of separating particles based on a combination of susceptibility and density.

Keywords: fine particle processing; magnetic separation; dense medium separation; mineral processing

1. Introduction

Magnetic separators exploit the difference in magnetic properties between the minerals and are used to separate valuable minerals from non-magnetic gangue, e.g. magnetite from quartz [1]. The same objective is often

----------*liushixiao8@hotmail.com

achieved in a very different way, the common features being a competition between a wide spectrum of forces of various magnitudes and ranges [2]. This method can be widely used in many areas such as in the separation of slurry mixed with a fine powder of α-hematite [3], physical coal cleaning [4], removal of aerosols from waste water [5], the treatment of landfill [6] and so on[7-9]. However, these techniques are restricted to treat ferromagnetic substances as the separation criteria are based on the repulsion/attraction in a magnetic field [10].

Since Beaugnon and Tournier succeeded in levitating water and some diamagnetic materials in 1991 [11], magnetic levitation has become one of the interesting topics in high magnetic field science where the diamagnetic levitation of bismuth [12] and the stable levitation of living frogs [13] has been reported. It has also been extended to investigate the growth of ionic crystals in a levitated solution and the levitation of molten glass without a crucible [14].

AVCO Corporation and NASA (USA) pioneered the use of ferrohydrostatic separators (FHS) in 1973 by employing a kerosene-based ferrofluid to separate automobile scrap [15].

Over the past decade a considerable amount of research has been conducted at the University of Nottingham on the levitation of particles under high magnetic gradients [16-18]. Building on previous results, this paper reports on the work conducted in separating streams of particles and minerals by horizontal deflection in paramagnetic fluids. The results show the potential of this approach to separate materials through a combination of density and/or susceptibilities.

2. Experimental procedure

2.1 Materials

2.1.1 Paramagnetic liquid

The magneto-Archimedes solution used in this chapter is $MnCl_2$ solution. Different concentrations of $MnCl_2$ solution were prepared (ie, 2 M, 3 M and 4 M) by dissolving the $MnCl_2$ crystal in distilled water to get a clear pink solution.

The mass susceptibility of the $MnCl_2$ solution at 2 M, 3 M, 4 M can be obtained by calculation from Andres (1975) [19], which stated that the mass susceptibility of an aqueous solution of a paramagnetic salt could be obtained from the formula below[19]:

$$x_{total} = C_{salt} x_{salt} + (1 - C_{salt}) \times x_{water} \quad (1)$$

$$C_{salt} = \frac{m_{salt}}{m_{total}} \quad (2)$$

The susceptibilities of $MnCl_2$ x_{salt} and water x_{water} are given as 114×10^{-6} and -0.724×10^{-6} $cm^3.g^{-1}$ in cgs Units respectively [19-22]. The volume susceptibility(k) of a 2M $MnCl_2$ solution can be obtained by satisfying the following formulas as below:

$$x_{salt} = \frac{m_{salt} x_{salt} + m_{water} x_{water}}{m_{salt} + m_{water}} \quad (3)$$

$$k = \rho x \times 4\pi \times 10^{-3} \quad (4)$$

The corresponding volume magnetic susceptibility of 2 M, 3 M and 4 M $MnCl_2$ solution were calculated and summarised in **Table. 1**.

2.1.2 Ore mineral particles

Ore mineral materials were prepared and investigated about the separation efficiencies in this paper. They were nickel ore located at Australia, copper ore A located at South Africa and copper ore B located at Atacama Desert, Northern Chile. These particles were crashed to the various size fractions needed in experiments by Retsch milling. MLA (Mineral Liberation Analyser) was used to quantify mineralogical characteristics of each kind of ore minerals.

The mineralogy compositions of the three kinds of ore samples obtained by MLA are listed in the following tables: **Table.2** (nickel ore), **Table.3** (copper ore A) and **Table.4** (copper ore B). The magnetic susceptibility values from various references are to give understanding how strong paramagnetic the mineralogy is.

2.1.3 The preparation and properties of run-of-mine coal samples

The run-of-mine coal used in this paper is Bituminous coal [24]. Bituminous coal is a soft, dense, black coal. Bituminous coal is used for generating electricity, making coke, and space heating and has calorific values ranging from 6.8 - 9 kW/kG approximately [25].

2.2 Superconducting magnet

The experiments were performed using an Oxford Instruments Minimum Condensed Volume (MCV) superconducting magnet, which had a 5cm diameter open bore with the maximum magnet central field being about 17 Tesla in the magnet bore, and the maximum BdB/dZ field gradient about $\pm$ 1470 T^2m^{-1}. The picture of the superconducting magnet is shown in **Fig. 1a**. The maximum field strength position is about 19cm down into the bore from the top plate of the superconducting magnet. The magnetic field strength plot is shown in **Fig. 1b**.

2.3 Design of glass box

As mentioned in our previous research work, the particles levitated in the Magneto-Archimedes fluid were repulsed to the wall of a container in the superconducting magnet field centre area.

In order to explore this interesting behaviour a rectangular glass box was made with dimensions, 145 x 195 x 25mm (**Fig. 2a**). The box was placed on top of the magnet with one of the end faces being positioned over the centre of the magnet bore. This was the point where the particles were fed or introduced in the fluid. Besides that, a collector was designed to be installed in the container and capture deflected particles as shown in **Fig. 2b**. The collector was put into the box during the experiment. After the particles were fed in, separation occurs (under the influence of the forces mentioned above) and they settle at different positions on the collector. The collector was then extracted from the container. The particles were collected from the collector based on several zones which depends on the distance from the magnet bore for analysis. For example, the zone of 0-40 mm means that the area on the collector is from the edge of zero mm distance to 40 mm distance from the magnet centre displayed **Fig. 2b**.

2.4 Heavy liquid analysis

After removing from the collector, the mixture of particles on every zone of the collector was separated by putting it into the solution of sodium polytungstate (SPT). The density of SPT solution was set to 3100 $kg.m^{-3}$ so the sand particles in it floated and the pyrite in it sank to the bottom. The density of the SPT can be increased by vaporizing or decreased by adding distilled water. In this way, the sand with a density 2650 $kg.m^{-3}$ and pyrite with a density around 4654 $kg.m^{-3}$ were separated and measured about the weight percentages.

3. Results and discussion

3.1 Effect of magnetic field and particle size

The size of particles and strength of the magnetic field are important factors to be investigated for the potential application of this technology. A series of experiments was carried out to study the effect of the magnetic field and particle size on the separation of pyrite and sand. During the experiments, the mixture of pyrite and sand (total 10g) with size fraction 0.15-0.6 mm were fed in to the experimental setup illustrated in **Fig. 2a**. The results are shown in **Fig. 3** and **Fig. 4** after heavy liquid analysis using SPT. Pyrite particles settled at the 0-40mm zone due to their high density and paramagnetism, their data were not included in the graphs. So if more sand particles were deflected away from the 0-40mm zone, better separation can be achieved. It can be seen from **Fig.3** that the effect of particle size (0.15-0.6mm) on the separation of sand and pyrite was negligible.

However, the intensity of magnetic field had a strong influence on the separation of particles as shown in **Fig. 4**. It is possible that at a field strength of 9.5 T the sand and pyrite particles all stayed in the 0-40 mm zone so were mixed and could not be separated. Most of the sand particles were deflected into the 40-80 mm zone at 12.5 T, in this case, there was some separation of the sand and pyrite particles. When the field strength increased to 16.5 T, the sand particles were deflected to a position far from the magnet bore whilst the pyrite particles were not deflected. This resulted in a complete separation of the sand and pyrite particles.

3.2 Effect of feeding positions on particle separation

In order to optimize the operating parameters to achieve better separation, several experiments were carried out to determine the effect of the feeding position on separation. In these experiments, the injector tube is inclined to form an angle with the top board surface of the magnet as shown in **Fig. 5**. The angle (α) was defined as the angle between the tube and the top board surface of the magnet. The velocity of particles as they leave the tube should be zero. The end of the injection tube was above 4M $MnCl_2$ solution surface. The injection distance shown in **Fig. 5** is half of the glass box length.

As the inclined injection tube was pointing to the magnet bore, the particles would drop to the zone of the collection system which was quite close to the magnet bore centre without the magnet field. The results of sand particles deflection was shown in **Fig. 6**, it could be indicated that the effect of feeding position on the sand particles deflection was negligible, as more than 99% of sand particles were deflected far away from the magnetic bore centre by 3 different feeding methods.

3.3 Experiments of ore samples

The behaviours of particles from several ore samples were examined in the superconducting magnetic system. SPT was used to analyze the distribution of particles in sink and float products at this stage. To investigate the effect of size fraction of particles on the separation efficiency, MLA was applied also.

3.3.1 Deflection of minerals under different magnetic field intensity

Magnetic field intensity shows paramount influence on the deflection of particles as per previous work. Experiments had been carried out to investigate the effect of magnetic field intensity on 3 kinds of ore samples, the results of SPT (whose density was set as 3000 $kg.m^3$) analysis on sink and float products were shown in **Fig. 7** – **Fig. 12**. It can be seen from **Fig. 7** that the compositions with lower density in copper ore B mineral particles (mainly quartz, illite and pyrophyllite) could be deflected away from magnetic bore centre (settling at 135-185mm zone) under 14.5 T and 16.5 T, but there were no heavier particles (mainly pyrite) settling at this zone. However, most of the particles (sulphides and gangues) would mix together if the intensity of magnetic field was lower than 14.5 T, thus it could not be separated. It could be concluded that major sulphides (pyrite, chalcocite group and covellite) could be separated from gangues such as quartz and illite among copper ore B sample as per the data in **Table. 4** and SPT results in **Fig. 7** and **Fig. 8**.

The results of nickel ores separation are shown in **Fig. 9** and **Fig. 10**. It is obvious that the sink and float particles all stayed in the same area and mixed together under four different magnetic field intensities. From **Table.2**, the main compositions in nickel ore are strong paramagnetic mineralogy (mainly hornblende, pentlandite, pyrrhotite). However, the metallic (mainly magnetite, olivine) and non-metalic (mainly calcite and dolomite) ores among copper ore A samples could be separated as per **Fig. 11** and **Fig. 12**. It can be seen from **Fig. 11** and **Fig. 12** that the particles had been well separated under 14.5T and 16.5 T, as some non-metalic particles (mainly calcite and dolomite) had

been deflected far away from magnetic bore centre (110-185mm zone, **Fig. 11**), but particles with higher density such as magnetite and olivine were attracted and settled at 0-40mm zone (**Fig. 12**).

3.3.2 Effect of particle size on deflection

Particle size is an important factor when it comes to the processing of ore minerals. The different size fractions of the ore samples ranging from 0.106mm to 3mm were investigated and the results after SPT analysis are shown in **Fig. 13** and **Fig. 14** (copper ore B), **Fig. 15** and **Fig. 16** (nickel ore), **Fig. 17** and **Fig. 18** (copper ore A).

It seemed the size fraction of particles (investigated range +0.106-3mm) showed negligible effect on the separation of copper ore B sample according to the data in **Fig. 13** and **Fig. 14**. Most of the metallic minerals (mainly pyrite, chalcocite) were settled at the 0-30mm zone close to magnetic bore centre, but the gangue minerals (quartz, illite and pyrophyllite) were deflected to the 100-185mm zone away from the centre, thus there was a clear boundary between these two parts and the particles could be completely separated. It is clearly seen from **Fig. 15** and **Fig. 16** that nickel ore mineral particles could not be effectively separated even changing the size fraction of particles. This may be ascribed to the fact that the main compositions among nickel ores are ferromagnetic (hornblende, pentlandite, pyrrhotite), and the ferromagnetic particles had so strong magnetic property (include Fe) that other diamagnetic particles (mainly talc and dolomite) had no chance to escape to the further end of the narrow glass box even when the particle size fraction was as small as 106 μm.

The results of copper ore A samples were shown in **Fig. 17** and **Fig. 18**, it can be seen that there was a clear boundary between high density paramagnetic particles which were mainly composed of magnetite and olivine (settling at 0-35mm zone) and lower density diamagnetic particles which were mainly composed of calcite and dolomite (deflected and settling at 100-185mm zone) under certain conditions. The interesting thing was good separation could be obtained when the particle size was a bit finer (+0.106-0.5mm), however, when the size of particle increased to about 0.71mm or coarser, the separation would worsen. This could be explained as the paramagnetic particles (magnetite and olivine) beginning to influence the movements of diamagnetic particles (calcite and dolomite) when particle size increased. When the particle size range increased to about 3 mm, the diamagnetic particles were not deflected at all but preferred to stay together with the paramagnetic particles. The

reason was hypothesized to be that when the big paramagnetic particles were attracted to the magnet bore centre, the other diamagnetic particles could not escape but being pushed down to the bottom with paramagnetic particles. When the size of particle decreased, the paramagnetic particles became much smaller, the gap among the paramagnetic particles were increased. In that way, the diamagnetic particles got more gaps and chances to escape so they could be deflected far away from the magnetic bore centre.

The fractions of ore mineral particles with size 0.25-0.5 mm and 2-3 mm along the collector before the SPT analysis were characterized by mineral liberation analyser (MLA) to obtain the MLA images and mineralogy compositions. The affect of size fraction on the magnetic horizontal deflection separation efficiency could be observed in more details and more clear by dividing the mineralogical compositions of ore minerals into two groups. One group is called relatively magnetic (rel_magnetic) and another group is called relatively diamagnetic (rel_diamagnetic) compared with 4 M $MnCl_2$ solution. The definition of two groups of mineralogy is based on the **Table.2**, **Table.3** and **Table.4**. The mineralogy which has stronger paramagnetic susceptibility and higher density compared with 4 M $MnCl_2$ solution in the tables can be called rel_magnetic. Other particles could be named rel_diamagnetic. In rel_diamagnetic group, the mineralogy which has weight percentage less than 5% can be summarised into “others” group. It should be noticed that the MLA method has a limitation that the results are based on two-dimensional analysis (the polished and carbon coated cross section of hardened round or square mould). The results do not include all of the particles but only the particles on the cross section. But it still can give a lot of information about the effect of size fraction on separation efficiency.

The MLA images of the copper ore B particles with different size fractions (0.25-0.5 mm, 2-3 mm) were showed in graph **Fig.19** and **Fig.20**. The particles with red colour were summarized as rel_magnetic and the particles with green colour were summarized as the rel_diamagnetic.

There is no particle at the 30-100 mm area when the size fraction of copper ore B is as high as 2-3 mm so there is no image of the sample at that specific area. Although the particles in copper ore B

were grouped to rel_magneitc and rel_diamagneitc, the mineralogy composition of the two groups could still be achieved and listed in the **Table.5** and **Table.6**.

The combination of **Fig. 19** and **Table.5** revealed that most particles with higher density and/or paramagnetism were settled at 0-100 mm zone especially in 0-30 mm zone, inversely the particles with lower density were deflected and settled at 100-185 mm zone which is far from magnetic bore centre. Compared with **Fig.19** and **Fig.20**, the separation can be achieved better when the size fraction of copper ore B is bigger.

The MLA images of the nickel ore particles with different size fractions (0.25-0.5 mm, 2-3 mm) were showed in below graphs **Fig.21** and **Fig.22**. The mineralogy (%wt) per fraction were listed in the **Table.7** and **Table .8**. It is displayed that the particles in nickel ore could not be separated well in **Fig. 21** and **Fig. 22**. Even though, the relatively paramagnetic particles such as pyrrhotite, magnetite, chromite still settled at the position which is near magnet bore centre area (0-30 mm). At the same time, the rel_diamagnetic particles were deflected a little bit from rel_magnetic particles which can be seen from **Table.7**. The weight percentages of rel_diamagnetic particles at 30-100 mm area are a little bit more than the corresponding 0-30 mm area.

The MLA images of the copper ore A particles separation results with different size fractions (0.25-0.5 mm, 2-3 mm) were showed in graphs **Fig.23** and **Fig.24**. The mineralogy (%wt) per fraction of copper ore A samples were listed in the **Table.9** and **Table .10**.

From **Fig.23**, **Fig.24**, **Table. 9** and **Table .10**, the relatively magnetic particle (mainly magnetite and biotite) can be separate effectively from relatively diamagnetic particles (mainly dolomite and apatite) when the size fraction is small. When the size fraction increased to 2-3 mm, the particles were mixed together and could not be separated effectively.

SPT analysis and MLA results demonstrate above indicate that particles with different density and/or susceptibility in real ore minerals could be settled at a certain position on the container floor due to the

unbalanced horizontal driving force, thus could be explored to separate particles under certain conditions.

3.4 Deflection of run-of-mine coal particles

From the above experiment results, it can be seen that the magnetic horizontal deflection has potential in the separation of sand and pyrite particles system, and some kinds of ore mineral particles system. The further exploration about the usage of magnetic horizontal deflection in the separation of run-of-mine coal particles was described in this section.

3.4.1 The choose of coal particles for experiments

The coal samples investigated in this paper were chosen to be the run-of-mine coal particles. The run-of-mine coal particles were treated to get rid of slurry first by washing with water. And then the size fraction of run-of-mine coal particles was chosen to be +1-3 mm diameter. The reason to choose the bigger size fraction is that the coal particles with fine size fraction would be dispersed in agent solution without settling down at the bottom of the chamber box.

3.4.2 Run-of-mine coal particles separation

The run-of-mine coal particles with size fraction +1-3 mm were prepared to 20 grams, 30 grams and 40 grams randomly and individually fed into 2 M $MnCl_2$ solution in the narrow glass box described before by a small tube under the high magnetic field strength where Bc=16.5 T. Every sample was tested three times. It can be seen clearly that the run-of-mine coal particles were separated into two streams which one of them stayed at the position near the magnet bore centre, another one were deflected to the further end of the glass narrow box. Very few amount particles settled at the central area of the bottom of the glass box. The mass distribution of the coal particles were showed in **Fig.25**.

The particles which settled at the area of 0-60 mm and 150-185 mm were collected and were measured about the density by Accupyc 1330 helium pycnometer and ash contents by burning in furnace for 2 hours. The results are shown in **Fig.26** and **Fig. 27**.

The graphs **Fig.26** and **Fig.27** show that the different density and ash content particles in run-of-mine coal were separated effectively. The particles which have density about 2600 $kg.m^{-3}$ in the run-of-

mine coal samples stayed at the area near the magnet bore centre, at the same time, the coal particles with about 1400 kg.m^{-3} density were deflected to the further end of the narrow glass box from the magnet bore centre. The particles with density about 2600 kg.m^{-3} have around 80% ash percent and particles with density 1400 kg.m^{-3} have 6% ash percent accordingly. In this case, the relatively pure coal particles which have lower density and lower ash contents can be separated from the other mineral particles in the sample.

The measurement results in graphs **Fig.26** and **Fig.27** were based on the 0-60 mm and 150-185 mm area of the bottom of the chamber box. Because the weight amount of the coal particles at the central area of the bottom of the glass box was not enough to be measured about the density and ash contents. To investigate the detailed separation efficiency of the particles at the central area of the glass box bottom again, the run-of-mine coal particles from the same sample source as before were treated to get rid of the particles density higher than 2600 kg.m^{-3} and particles density lower than 1400 kg.m^{-3} by SPT (high density fluid) 'sink and float' method. The remain particles whose density were between 1400 and 2600 kg.m^{-3} were also prepared as 20 g, 30 g and 40 g randomly and feed into 2 M $MnCl_2$ solution. The settle down positions of these particles along the bottom of the narrow glass box were explored. The results about mass distribution, densities distribution and ash contents distribution were showed as below **Fig.28**, **Fig.29** and **Fig.30**.

There were no particles at all in the central area of the bottom of the narrow glass box from the above **Fig. 28**, **Fig. 29** and **Fig. 30**. The particles with different density about 2500 and 2000 kg.m^{-3} were separated effectively. In **Fig. 29** and **Fig. 30**, the particles with density about 2500 kg.m^{-3} settled at the position near the magnet bore centre which is the same zone with 2600 kg.m^{-3} density particles, the particles with density 2000 kg.m^{-3} were deflected to the area further away from magnet bore centre which is the same zone with 1400 kg.m^{-3} density particles. The compositions with different densities in run-of-mine coal materials can be separated effectively by magnetic horizontal deflection.

4. Conclusions

When streams of particles with different parameters such as sand and pyrite, ore samples and run-of-mine coal particles were put in the same magnetic system, similar results were obtained as that of a single particle. Particles with different density and susceptibility settled down at different positions on the container floor due to the combined forces of gravity and magneto-Archimedes as well as a lateral buoyancy (displacement) force.

Good results had been obtained during the separation of model minerals (pyrite and sand), however, when it comes to the real ore samples, the separation efficiency would depend on the property and complexity of ores. It was found that nickel ore sample could not be well separated as per the experimental results, this was partly due to the entrainment of strong magnetic property particles (mainly amphibole, pyrrhotite, pentlandite) during its attraction to the collector bottom which blocked the deflection of diamagnetic particles. In order to solve this problem, pre-treating of materials (magnetic separation) to remove magnetic particles is necessary in the future work.

Besides that, the compositions with different densities or ash contents in run-of-mine coal particles can be effectively separated. The higher density compositions in run-of-mine coal particles with higher ash contents prefer to stay at the area where is quite near the magnet bore centre. The lower density particles with lower ash contents were repulsed to the further end of the narrow glass box.

The method potentially could be further developed for the separation of particles as per susceptibility and/or density and recovery of metal and plastic from waste printed circuit board.

Acknowledgements

This work was funded as part of the UK Engineering and Physical Sciences Research Council Basic Technology Programme: Magnetic Levitation Technology for Mineral Separation, Nanomaterials, and Biosystems for Space Exploration (GR/S83005/01)

NOMENCLATURE

Variables

B	the magnetic induction field strength	(T)
C_{salt}	mass percentage of salt in the total mass	(-)
g	the acceleration of gravity	(m/s^2)
k	volume magnetic susceptibility	(-)
k_1 (or k_p)	mass susceptibility of the levitating substances	(-)
k_2 (or k_l)	mass susceptibility of the medium gas (or liquid)	(-)
m	the mass of the particle	(kg)
χ	mass magnetic susceptibility	(m^3/kg)
μ_0	the permeability of free space	(H/m)
ρ	mass density	(kg/m^3)
$\frac{dB}{dz}$	vertical direction magnetic field gradient	(T/m)

Reference

[1] Wills, B. A. and Napier-Munn, T. (2006), 'Mineral Processing Technology', *Elsevier Science & Technology Books*

[2] Svoboda, J. (2004), 'Magnetic Techniques for the Treatment of Materials', *Kluwer Academic Publisher*

[3] Yokoyama, K., Oka, T., Okada, H., Fujine, Y., Chiba, A. and Noto, K. (2003), 'Solid-Liquid Magnetic Separation Using Bulk Superconducting Magnets', *IEEE Transactions on applied superconductivity*, Vol. 13, No. 2, June, pp. 1592-1595

[4] Doctor, R. D. and Livengood, C. D. (1990), 'Open-Gradient Magnetic Separation for Physical Coal Cleaning: Results for Pittsburgh #8 and Upper Freeport Coals', pp. 228-235

[5] Okada, H., Okuyama, H., Uda, M. and Hirota, N. (2006), 'Removal of Aerosol by Magnetic Separation', *IEEE Transactions on Applied Superconductivity*, Vol. 16, No. 2, June, pp. 1084-1087

[6] Ihara, I., Kanamura, K., Shimada, E. and Watanabe, T. (2004), 'High Gradient Magnetic Separation Combined With Electrocoagulation and Electrochemical Oxidation for the Treatment of Landfill Leachate', *IEEE Transactions on applied superconductivity*, Vol. 14, No. 2, June, pp. 1558-1560

[7] Ito, D., Miura, K., Ichimura, T., Ihara, I. and Watanabe, T. (2004), 'Removal of As, Cd, Hg and Pb Ions From Solution by Adsorption With Bacterially- Produced Magnetic Iron Sulfide Particles Using

High Gradient Magnetic Separation', *IEEE Transactions on applied superconductivity*, Vol. 14, No. 2, June, pp. 1551-1553

[8] Okada, H., Kudo, Y., Nakazawa, H., Chiba, A., Mitsuhashi, K., Ohara, T. and Wada, H. (2004), 'Removal System of Arsenic From Geothermal Water by High Gradient Magnetic Separation-HGMS Reciprocal Filter', *IEEE Transactions on Applied Superconductivity*, Vol. 14, No. 2, June, pp. 1576-1579

[9] Hartikainen, T., Nikkanen, J. and Mikkonen, R. (2005), 'Magnetic Separation of Industrial Waste Waters as an Environmental Application of Superconductivity', *IEEE Transactions on Applied Superconductivity*, Vol. 15, No. 2, June, pp. 2336-2339

[10] Ikezoe, Y., Kaihatsu, T., Sakae, S., Uetake, H., Hirota, N. and Kitazawa, K. (2002), 'Separation of feeble magnetic particles with magneto-Archimedes levitation', *Energy Conversion and Management,* Vol. 43, pp. 417-425

[11] Beaugnon, E. and Tournier, R. (1991), 'Levitation of water and organic substances in high static magnetic fields", *Nature*, Vol. 349, pp. 470

[12] Braunbeck, W. (1939), 'Magnetic levitation of graphite', *Z. Physics*, Vol. 112, pp. 735.

[13] Berry, M. V. and Geim, A. K. (1997), 'Of flying frogs and levitrons', *The European Physical Society*, Vol. 18, pp. 307-313

[14] Mothokawa, M., Hamai, M. and Sato, T. (2001), 'Magnetic levitation experiments in Tohoku University', *Physica B*, Vol. 294-295, pp. 729-735

[15] Mir, L., Simard, C. and Grana, S. D. (1973), *Proc. 3rd Urban Technol. Conf. Tech. Display*, *Boston (USA)*, AIAA Paper no. 73-959

[16] Catherall, T. A., Eaves, L., King, J. P. and Booth, R. S. (2003), 'Floating gold in cryogenic Oxygen', *Nature*, Vol. 422, April, pp.579

[17] Catherall, T. A., Lopez-Alcaraz, P., Benedict, K. A., King, J. P. and Eaves, L. (2005), 'Cryogenically enhanced magneto-Archimedes levitation', *New J. Phys*. Vol. 7, pp. 118

[18] Lopez-Alcaraz, P., Catherall, A. T., Hill, R. J. A., Leaper, M. C., Michael R. Swift, M. R. and King, P. J. (2007), 'Magneto-vibratory separation of glass and bronze granular mixtures immersed in a paramagnetic liquid', *The European Physical Journal E*: *Soft Matter and Biological Physics,* Vol.24, pp. 145-156

[19] Andres, U. (1975), 'Magnetohydrodynamic and Magnetohydrostatic Separation - A new prospect for mineral separation in the magnetic field', *Mineral Science Engineering*, Vol. 7, No.2, April, pp. 99-109

[20] Suwa, M. and Watarai, H. (2002), 'Magnetophoretic Velocimetry of Manganese(II) in a Single Microdroplet in a Flow System under a High Gradient Magnetic Field Generated with a Superconducting Magnet', *Anal. Chem*. Vol. 74, pp. 5027-5032

[21] Rnstein, Landolt-B. (1986), 'Numerical Data and Functional Relationships in Science and Technology', *New Series, II/16, Diamagnetic Susceptibility, Springer-Verlag, Heidelberg*

[22] Arrighini, G. P., Maestro, M. and Moccia, R. (1968), 'Magnetic Properties of Polyatomic Molecules: Magnetic Susceptibility of H_2O, NH_3, CH_4, H_2O_2', *J. Chem. Phys.* Vol. 49, pp. 882-889.

[23] Bennett, L. H., Page, C. H. and Swartzendruber, L. J. (1978), 'Comments on units in magnetism', *Journal of Research of the National Bureau of Standards*, Vol. 83 (1), pp. 9-12

[24] Palmer, C. A. and Lyons, P. C. (1996), 'Selected elements in major minerals from bituminous coal as determined by INAA: implications for removing environmentally sensitive elements from coal', *International Journal of Coal Geology*, Vol. 32, pp. 151- 166

[25] Belkin, H. E., Tewalt, S. J., Hower, J. C., Stucker, J. D., O'Keefe, M. K. J., Tatu, C. A. and Buia, G. (2009), 'Petrography and geochemistry of oligocene bituminous coal from the Jiu Valley, Petrosani basin (southern Carpathian Mountains), Romania', *International Journal of Coal Geology*, doi: 10.1016/j.coal.2010.01.013

Particle separation by horizontal deflection in paramagnetic fluid

Figure captions:

Fig.1: MCV magnetic system used in experiments and the field gradient at top surface

Fig.2: Experimental setup and design of collector

Fig.3: Effect of particle size on separation of sand and pyrite

Fig.4: Effect of magnetic field intensity on separation of sand and pyrite

Fig.5: Scheme for particle dropping position

Fig.6: Sand distribution mass on different feed positions

Fig.7: Effect of magnetic field intensity on separation of copper ore B: particle distribution in float product

Fig.8: Effect of magnetic field intensity on separation of copper ore B sample: particle distribution in sink product

Fig.9: Effect of magnetic field intensity on separation of nickel ore sample: particle distribution in float product

Fig.10: Effect of magnetic field intensity on separation of nickel ore sample: Particle distribution in sink product

Fig.11: Effect of magnetic field intensity on separation of copper ore A sample: particle distribution in float product

Fig.12: Effect of magnetic field intensity on separation of copper ore A sample: particle distribution in sink product

Fig.13: Effect of particle size on separation of copper ore B sample: particle distribution in float product

Fig.14: Effect of particle size on separation of copper ore B sample: particle distribution in sink product

Fig.15: Effect of particle size on separation of nickel ore sample: Particle distribution in float product

Fig.16: Effect of particle size on separation of nickel ore sample: Particle distribution in sink product

Fig.17: Effect of particle size on separation of copper ore A sample: Particle distribution in float product

Fig.18: Effect of particle size on separation of copper ore A sample: Particle distribution in sink product

Fig.19: The MLA images of copper ore B sample (0.25-0.5 mm)

Fig.20: The MLA images of copper ore B sample (2-3 mm)

Fig.21: The MLA images of nickel ore sample (0.25-0.5 mm)

Fig.22: The MLA images of nickel ore sample (2-3 mm)

Fig.23: The MLA images of copper ore A sample (0.25-0.5 mm)

Fig.24: The MLA images of copper ore A sample (2-3 mm)

Fig.25: The mass percentage distribution of run-of-mine coal particles

Fig.26: The run-of-mine coal ash content percentage distribution results of 0-60 and 150-185 mm areas.

Fig.27: The run-of-mine coal density distribution results of 0-60 and 150-185 mm areas.

Fig.28: The mass percentage distribution of the run-of-mine coal particle whose density were between 1400 and 2600 $kg.m^{-3}$

Fig.29: The density distribution of the run-of-mine coal particle whose density were between 1400 and 2600 $kg.m^{-3}$

Fig.30: The ash content distribution of the run-of-mine coal particle whose density were between 1400 and 2600 $kg.m^{-3}$.

All the colour figures are intended for colour reproduction on the web and black-and-white in print.

a. MCV magnetic system

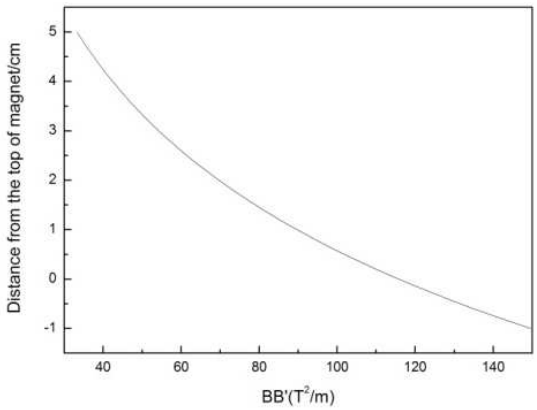

b. BB' versus distance from the top of magnet

Fig. 1: MCV magnetic system used in experiments and the field gradient at top surface

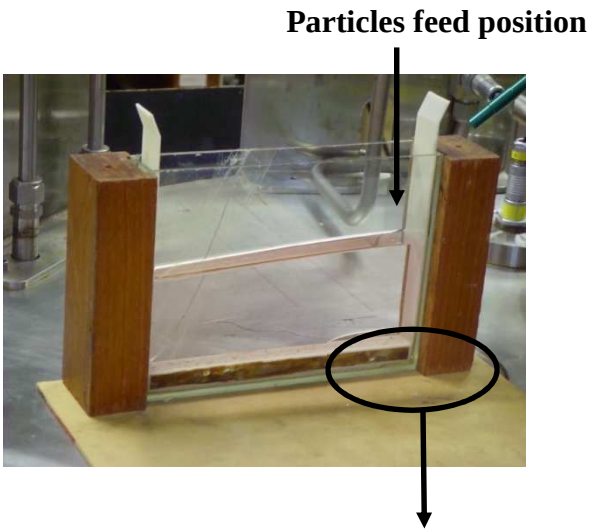

a. Experimental setup

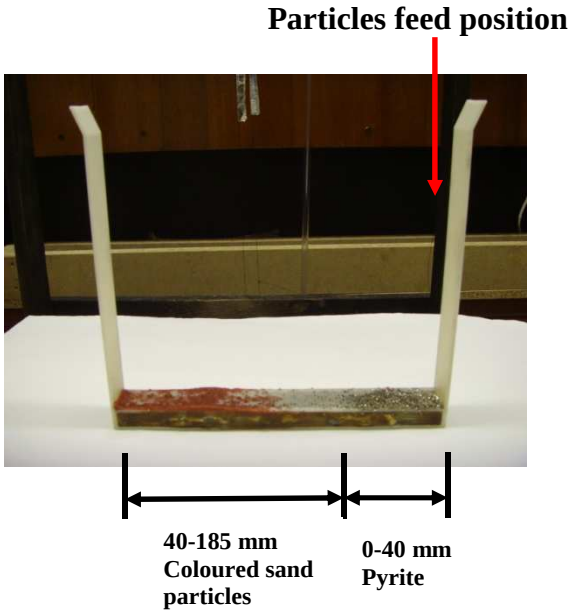

b. The design of collector

Fig. 2: Experimental setup and design of collector

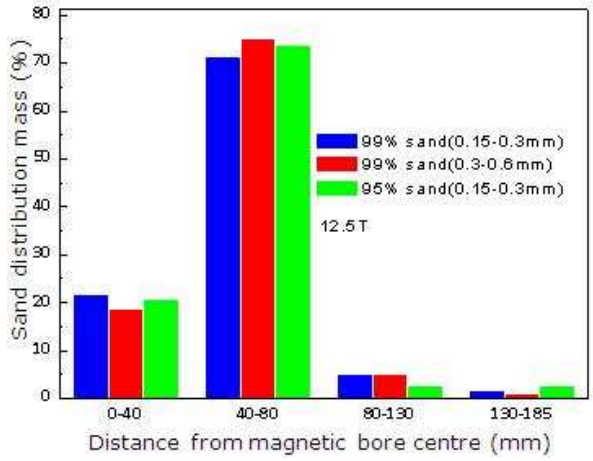

Fig.3: Effect of particle size on separation of sand and pyrite

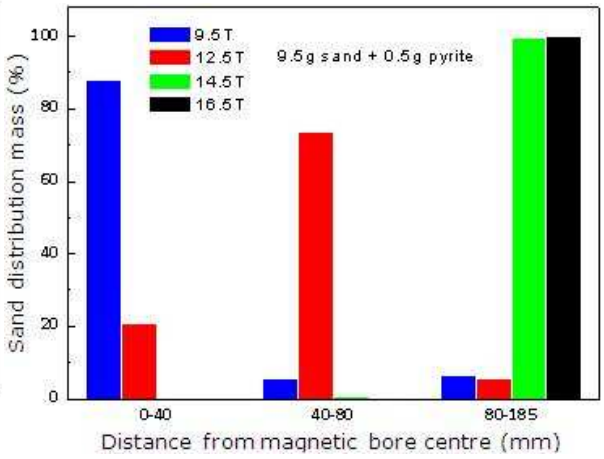

Fig. 4: Effect of magnetic field intensity on separation of sand and pyrite

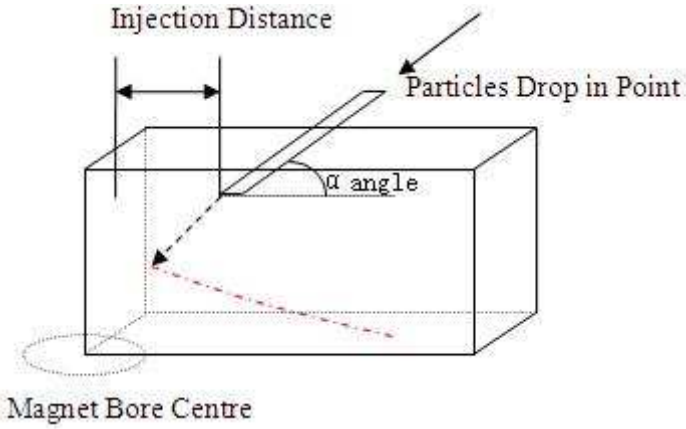

Fig.5: Scheme for particle dropping position

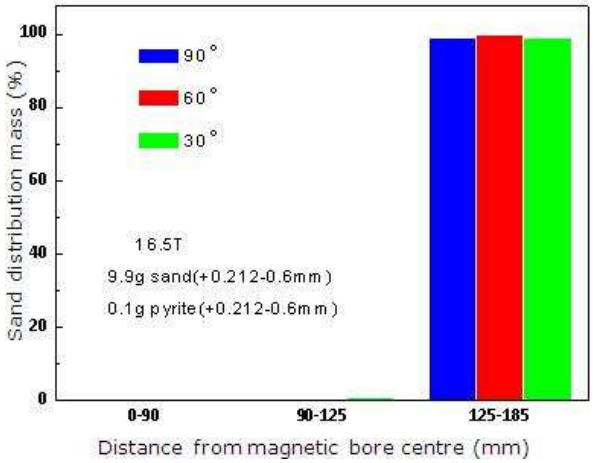

Fig.6: Sand distribution mass on different feed positions

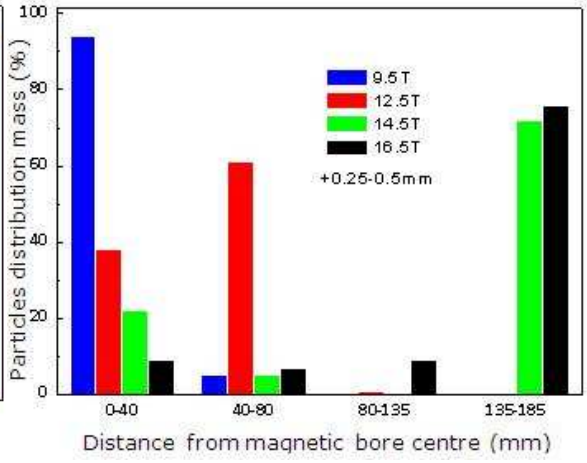

Fig.7: Effect of magnetic field intensity on separation of copper ore B: particle distribution in float product

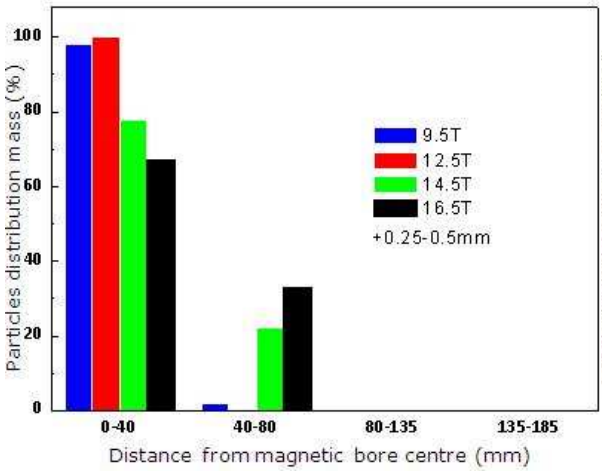

Fig.8: Effect of magnetic field intensity on separation of copper ore B sample: particle distribution in sink product

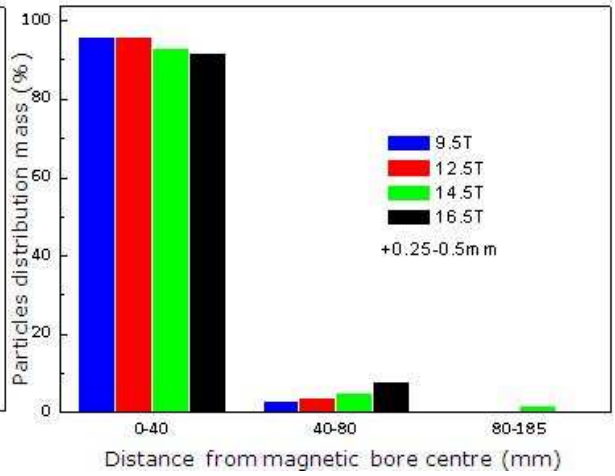

Fig.9: Effect of magnetic field intensity on separation of nickel ore sample: particle distribution in float product

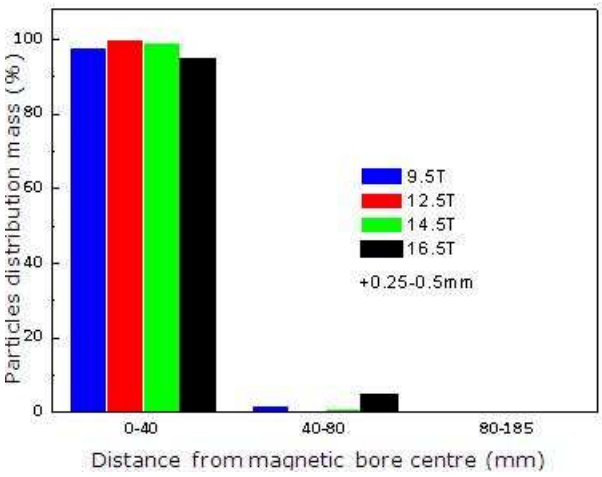

Fig.10: Effect of magnetic field intensity on separation of nickel ore sample: Particle distribution in sink product

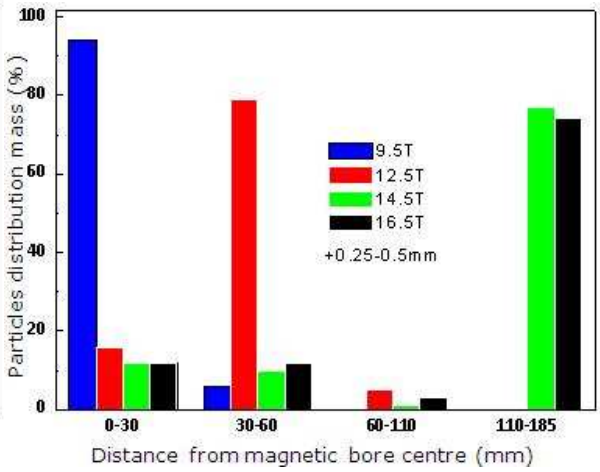

Fig.11: Effect of magnetic field intensity on separation of copper ore A sample: particle distribution in float product

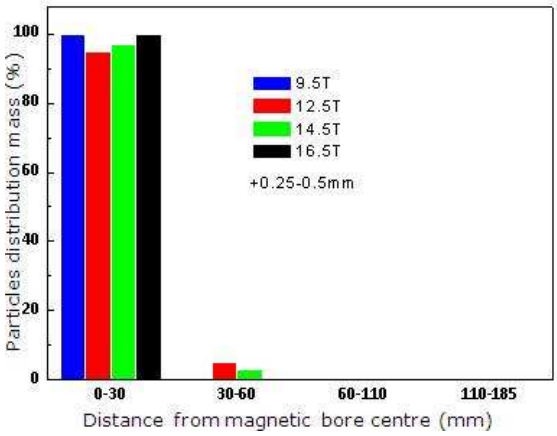

Fig.12: Effect of magnetic field intensity on separation of copper ore A sample: particle distribution in sink product

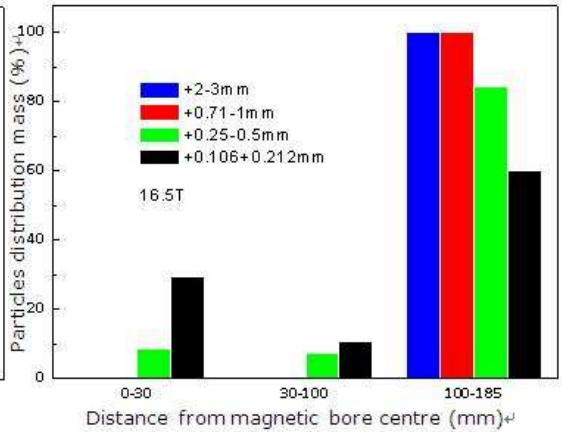

Fig.13: Effect of particle size on separation of copper ore B sample: particle distribution in float product

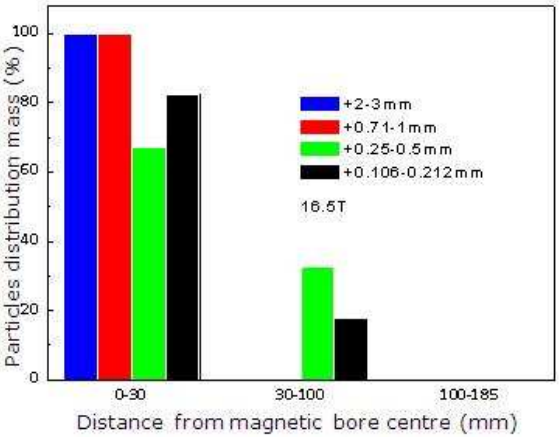

Fig.14: Effect of particle size on separation of copper ore B sample: particle distribution in sink product

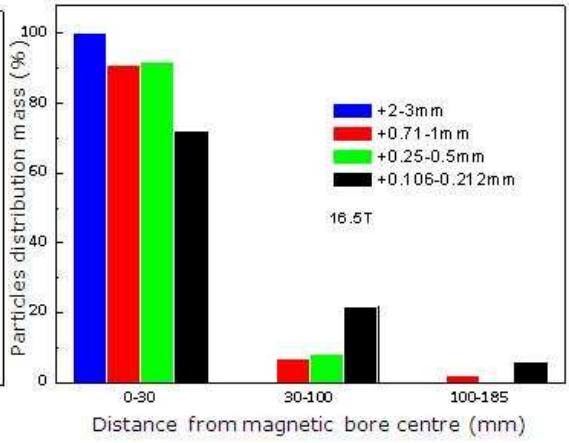

Fig.15: Effect of particle size on separation of nickel ore sample: Particle distribution in float product

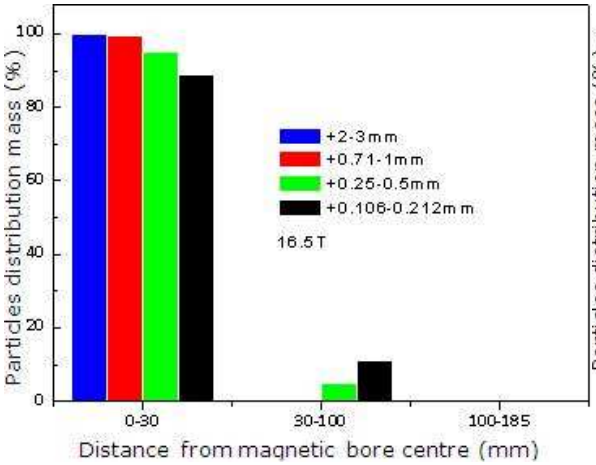

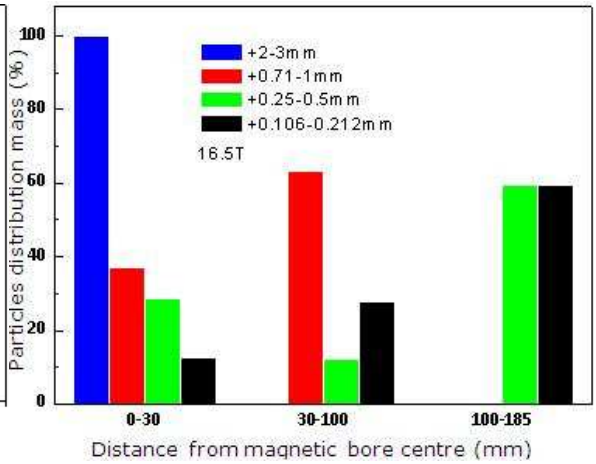

Fig.16: Effect of particle size on separation of nickel ore sample: Particle distribution in sink product

Fig.17: Effect of particle size on separation of copper ore A sample: Particle distribution in float product

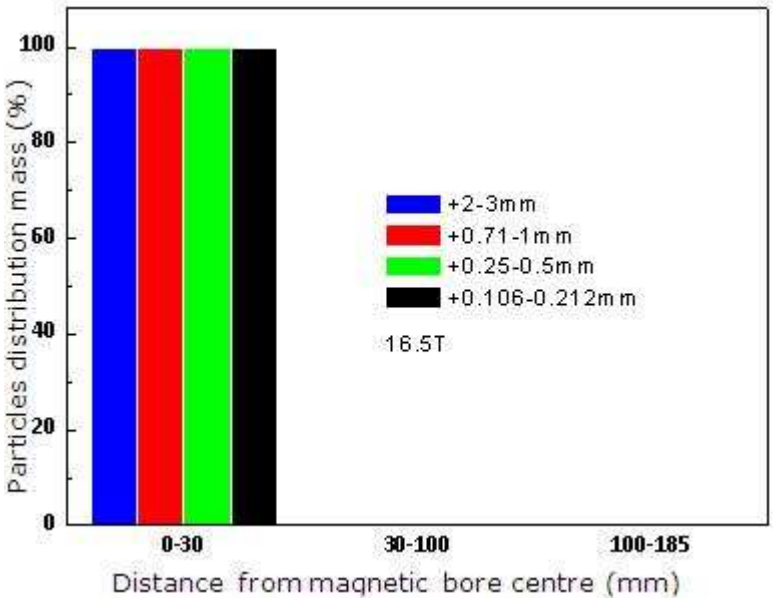

Fig.18: Effect of particle size on separation of copper ore A sample: Particle distribution in sink product

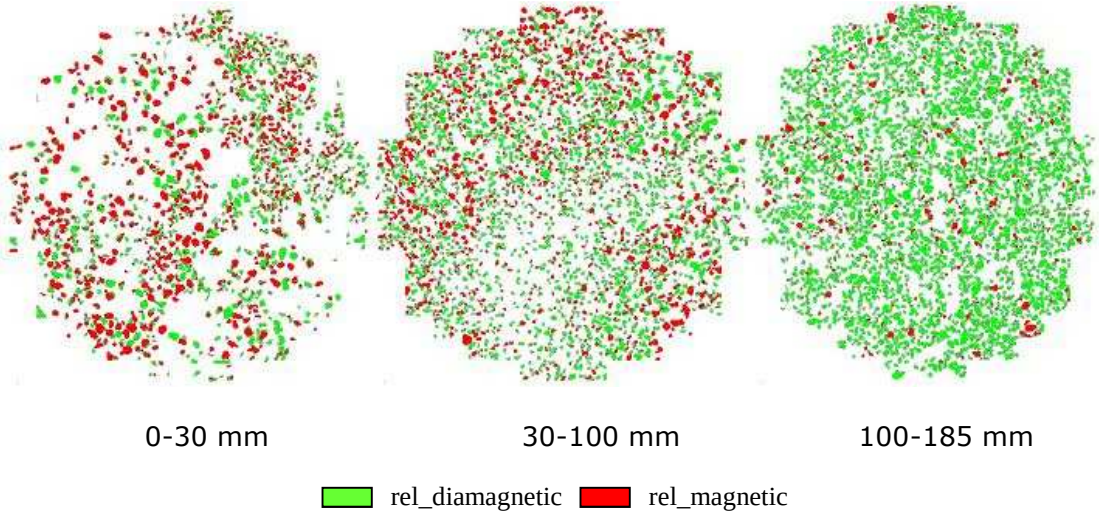

Fig.19: The MLA images of copper ore B sample (0.25-0.5 mm)

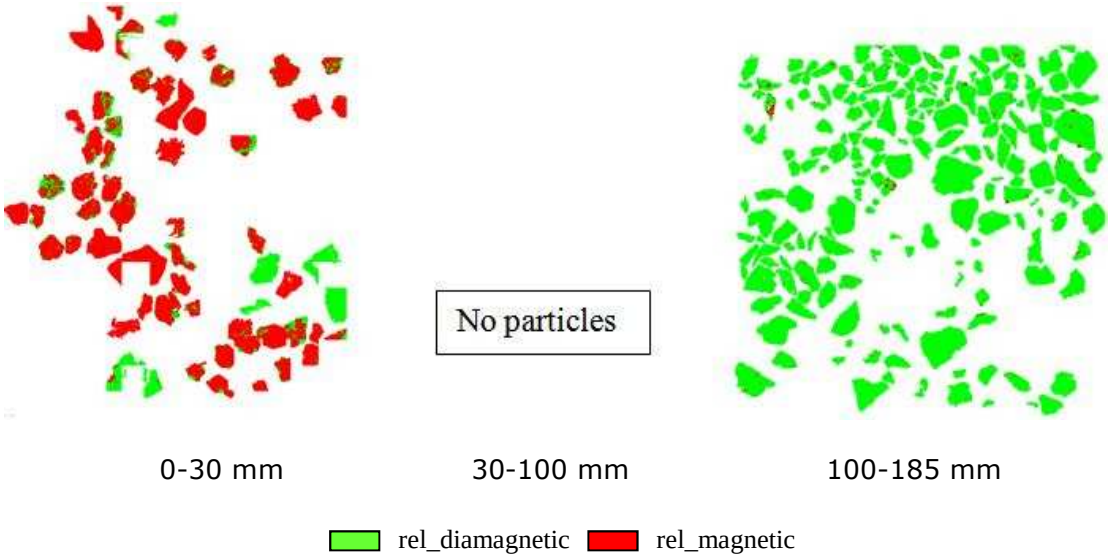

Fig.20: The MLA images of copper ore B sample (2-3 mm)

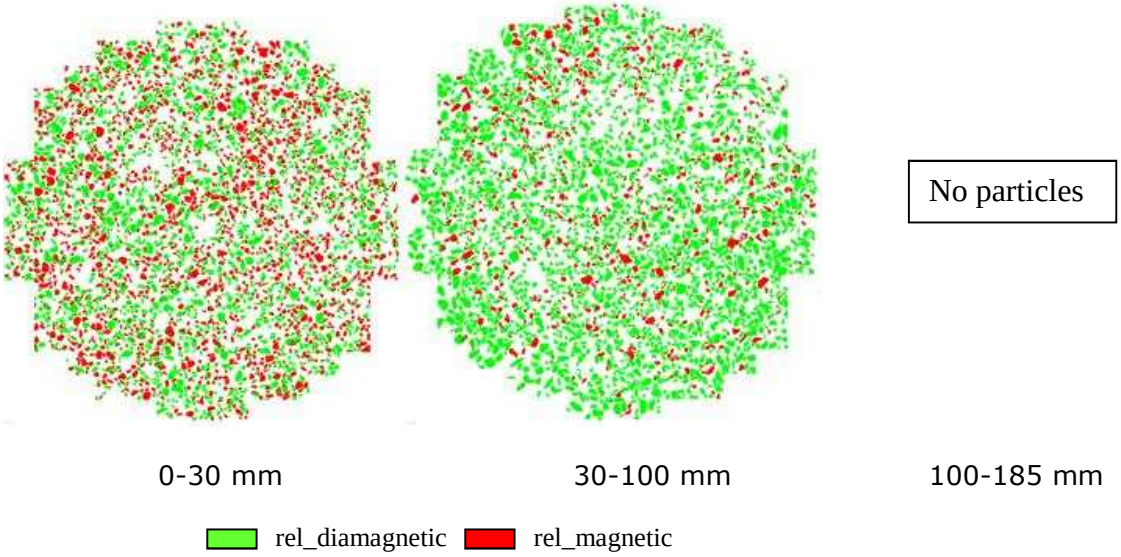

Fig.21: The MLA images of nickel ore sample (0.25-0.5 mm)

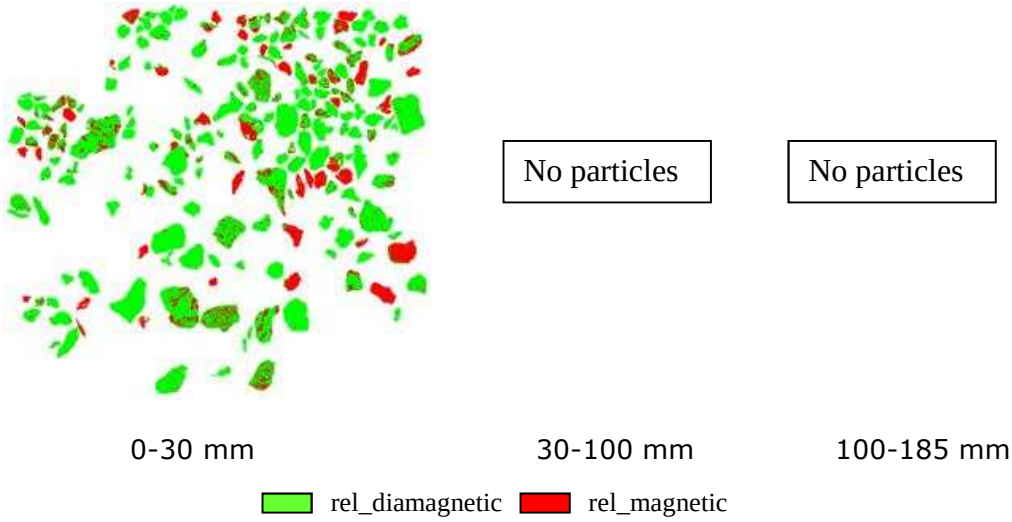

Fig.22: The MLA images of nickel ore sample (2-3 mm)

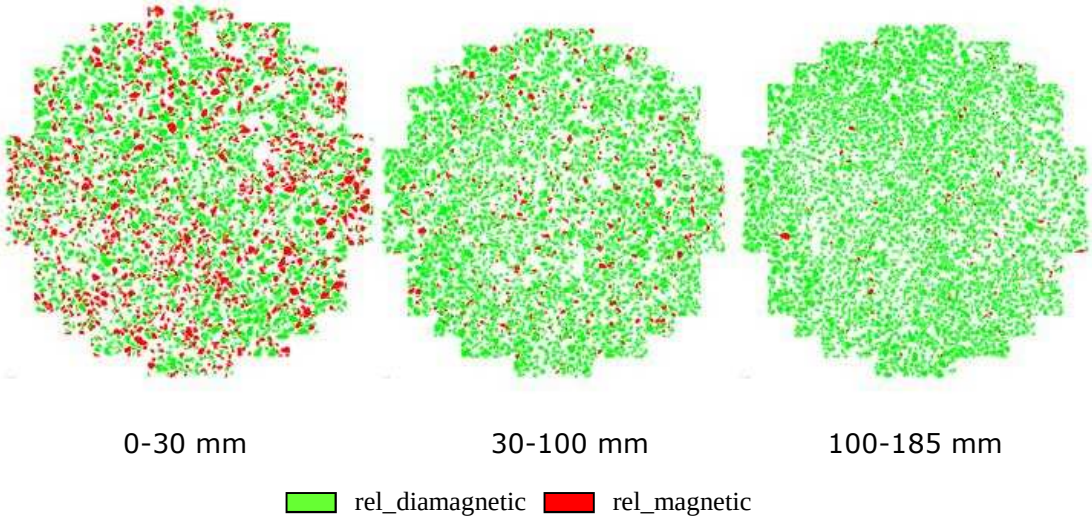

Fig.23: The MLA images of copper ore A sample (0.25-0.5 mm)

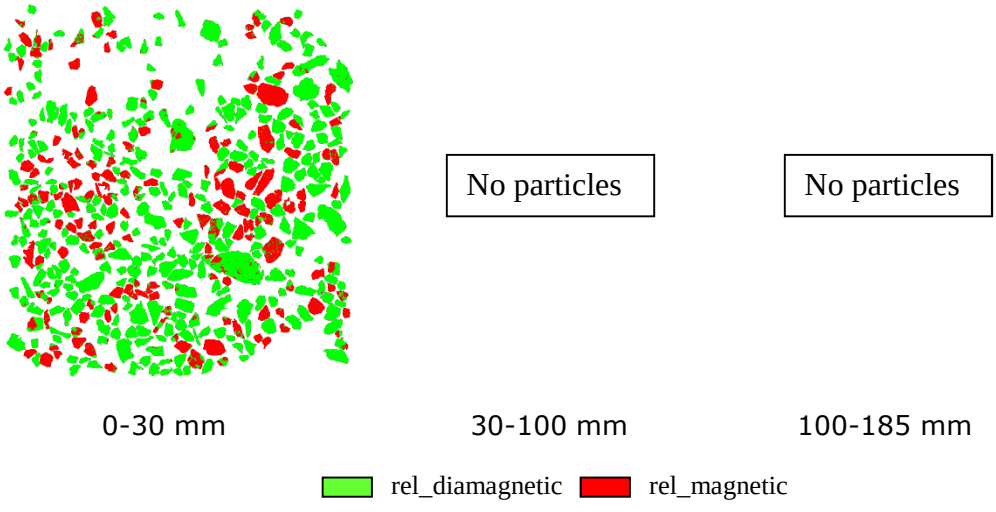

Fig.24: The MLA images of copper ore A sample (2-3 mm)

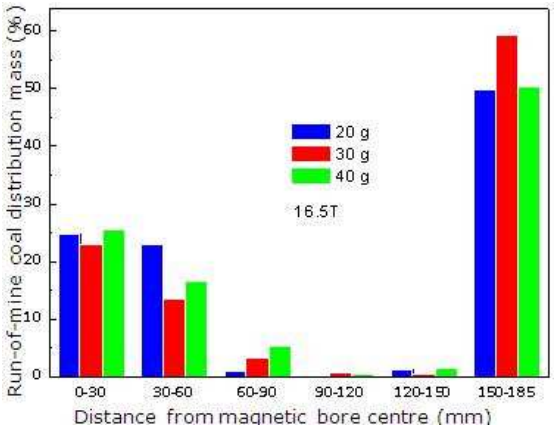

Fig.25: The mass percentage distribution of run-of-mine coal particles

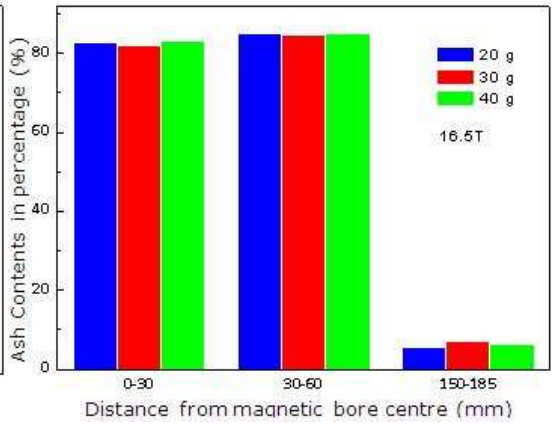

Fig.26: The run-of-mine coal ash content percentage distribution results of 0-60 and 150-185 mm areas.

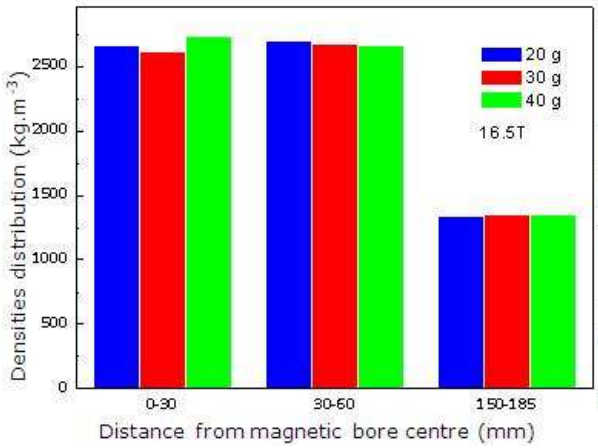

Fig.27: The run-of-mine coal density distribution results of 0-60 and 150-185 mm areas.

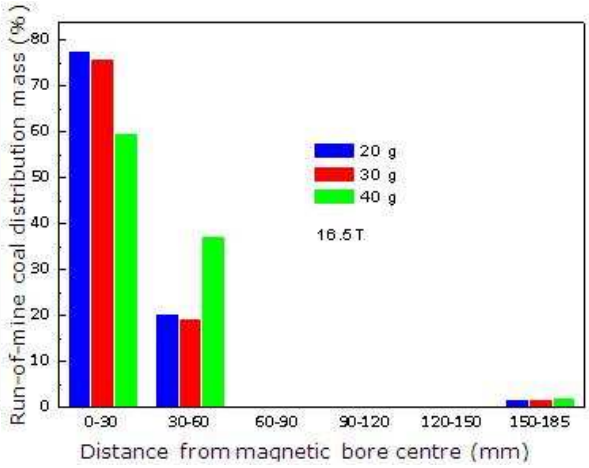

Fig.28: The mass percentage distribution of the run-of-mine coal particle whose density were between 1400 and 2600 kg.m^{-3}

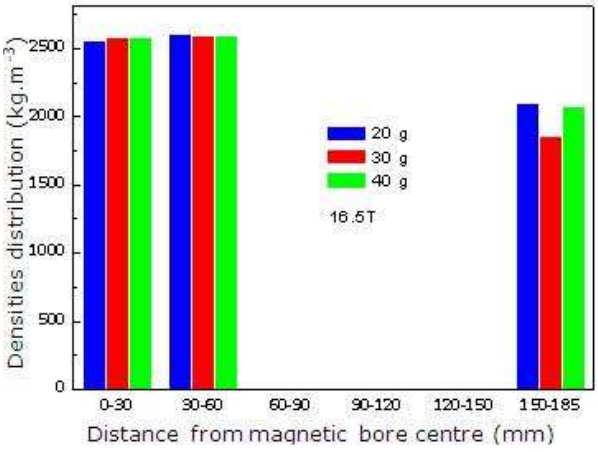

Fig.29: The density distribution of the run-of-mine coal particle whose density were between 1400 and 2600 kg.m^{-3}

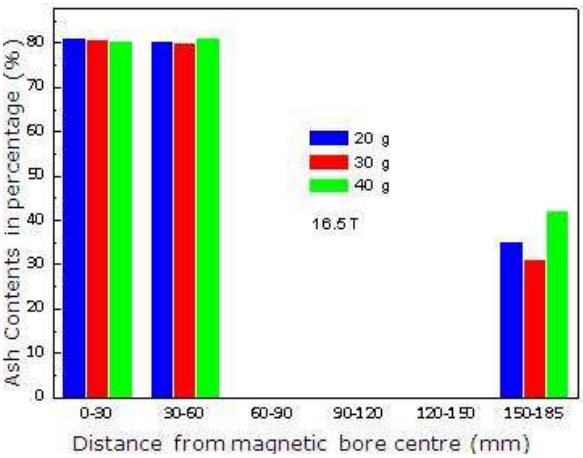

Fig.30: The ash content distribution of the run-of-mine coal particle whose density were between 1400 and 2600 kg.m^{-3}.

Particle separation by horizontal deflection in paramagnetic fluid

Table captions:

Table.1: The density and volume magnetic susceptibility of different concentrations manganese (II) chloride solution

Table. 2: The mineral properties in nickel ore [19, 26-32]

Table. 3: The mineral properties in copper ore A [19, 26-32]

Table. 4: The mineral properties in Copper ore B [19, 26-32]

Table. 5: The mineralogy (%wt) per fraction of copper ore B (0.25-0.5 mm) obtained by MLA

Table.6: The mineralogy (%wt) per fraction of copper ore B (2-3 mm) obtained by MLA

Table. 7: The mineralogy (%wt) per fraction of nickel ore (0.25-0.5 mm) obtained by MLA

Table. 8: The mineralogy (%wt) per fraction of nickel ore (2-3 mm) obtained by MLA

Table. 9: The mineralogy (%wt) per fraction of copper ore A (0.25-0.5 mm) obtained by MLA

Table. 10: The mineralogy (%wt) per fraction of copper ore A (2-3 mm) obtained by MLA

Table.1: The density and volume magnetic susceptibility of different concentrations manganese (II) chloride solution

Solution	Density ($kg.m^{-3}$)	k X 10^{-6}
2 M Manganese(II) Chloride	1227	345
3 M Manganese(II) Chloride	1301	502
4 M Manganese(II) Chloride	1395	660

Table. 2: The mineral properties in nickel ore [19, 26-32]

Compositions	Chemical Form	Density ($kg.m^{-3}$)	k_pX10^{-6}	X_p X 10^{-9} ($m^3.kg^{-1}$)	Fraction Percentages
Plagioclase	$(Na,Ca)(Si,Al)_4O_8$	2680	(-)	(-)	6.5
Albite	$NaAlSi_3O_8$	2620	-9.4	-3.6	5.12
Anorthite	$CaAl_2Si_2O_8$	2730	(-)	(-)	2.36
Quartz	SiO_2	2650	-15.1	-5.7	2.45
Talc	$Mg_3Si_4O_{10}(OH)_2$	2750	67.32	24.48	14.88
Calcite	$CaCO_3$	2710	-10.3	-3.8	2.62
Dolomite	$CaMg(CO_3)_2$	2974	45	15.1	5.94
Pyrite	FeS_2	4654	314	67.5	3.65
Magnetite	$FeFe_2O_4$	4740	Ferromagnetic	Ferromagnetic	1.9
Pentlandite	$(Fe,Ni)_9S_8$	4800	(-)	Paramagnetic	6.28

Pyrrhotite	$Fe_{(1-x)}S$ (x=0-0.17)	4610	(-)	Anti-ferro magnetic	8.84
Chalcopyrite	$CuFeS_2$	4250	6783	1596	0.72
Chromite	$(Fe,Mg)(Cr, Al)_2O_4$	5091	2953-5539	580-1088	0.49
Ilmenite	$FeTiO_3$	4720	453.12	96	0.23
Hornblende	(2.1% Fe)	2900-3500	9000	2500-3000	25.1
Chlorite	$(Mg_3,Fe_2)Al(AlSi_3)O_{10}(OH)_8$	3000	4673	1558	6.33
Biotite	$K(Mg,Fe)_3[Si_3AlO_{10}](OH,F)_2$	3020-3120	96-1180	32-378	3.99
Magnesite	$MgCO_3$	3000	-1.53	-0.51	2.26
Allanite	$CaAl_2(Fe++,Fe+++)(SiO_4)(Si_2O_7)O(OH)$	3930	(-)	(-)	0.02
Titanite	$CaTiSiO_5$	3480	(-)	(-)	0.27

Table. 3: The mineral properties in copper ore A [19, 26-32]

Compositions	Chemical Form	Density ($kg.m^{-3}$)	$k_p X10^{-6}$	χ_p X 10^{-9} ($m^3.kg^{-1}$)	Fraction Percentages
Hydrotalcite	$Mg_6Al_2(CO_3)(OH)_{16}•4(H_2O)$	2060	(-)	(-)	0.22
Calcite	$CaCO_3$	2710	-10.3	-3.8	29.39
Dolomite	$CaMg(CO_3)_2$	2974	45	15.1	6.26
Magnetite	$FeFe_2O_4$	4740	Ferromagnetic	Ferromagnetic	43.02
Chalcocite	Cu_2S	5700	(-)	(-)	0.34
Chalcopyrite	$CuFeS_2$	4250	6783	1596	0.02
Uranothorianite	$(Th,U)O_2$	(-)	(-)	(-)	0.04
Galena	PbS	7230	-31.8	-4.4	0
Bornite	Cu_5FeS_4	5070	664.17	131	0.04
MA_Spinel	$MgAl_2O_4$	3640	(-)	(-)	1.09
Valleriite	$4(Fe,Cu)S•3(Mg,Al)(OH)_2$	3110	(-)	(-)	0.36
Chlorite_ Group	$(Mg_3,Fe_2)Al(AlSi_3)O_{10}(OH)_8$	3000	4673	1558	0.22
Biotite	$K(Mg,Fe)_3[Si_3AlO_{10}](OH,F)_2$	3020-3120	96-150	32-48	0.91
Fluorite	CaF_2	3180	-2	-0.63	0.06
Apatite	$Ca_5(PO_4)_3(OH,F,Cl)$	3170-3180	-0.8	-0.26	7.46
Monazite	(Ce,La,Y,Th) PO_4	4900-5500	53-60	10.9	0.07
Baddeleyite	(Ce,La,Nd,Th) PO_4	5600	-0.62	-0.112	0.11
Serpentine_ Group	(-)	(-)	(-)	(-)	0.21
Olivine	$(Mg,Fe)_2SiO_4$	3320	Paramagnetic	Paramagnetic	10.2

Table. 4: The mineral properties in Copper ore B [19, 26-32]

Compositions	Chemical Form	Density ($kg.m^{-3}$)	$k_p X10^{-6}$	X_p X 10^{-9} ($m^3.kg^{-1}$)	Fraction Percentages
Illite	$(K,H_3O)(Al,Mg,Fe)_2(Si,Al)_4O_{10}(OH)_2(H_{20})$	2750	138.2	50.25	10.96
Kaolinite	$Al_2Si_2O_5(OH)_4$	2600	65	25	1.54
Pyrophyllite	$Al_2Si_4O_{10}(OH)_2$	2840	(-)	(-)	17.3
Quartz	SiO_2	2650	-15.1	-5.7	33.97
Albite_ oligoclase	$NaAlSi_3O_8$	2620	(-)	(-)	3.51
Smectite	(-)	2350	(-)	(-)	0.57
Gypsum	$CaSO_4\ 2H_2O$	2320	(-)	(-)	0.01
Chalcopyrite	$CuFeS_2$	4250	6783	1596	0.84
Bornite	Cu_5FeS_4	5070	664.17	131	0.62
Covellite	CuS	4700	(-)	(-)	1.27
Chalcocite_ group	Cu_2S	5700	(-)	(-)	3.7
Sphalerite	ZnS	4000	-13.2	-3.3	0.46
Galena	PbS	7500	-33	-4.4	0.02
Rutile	TiO_2	4200	50-215	12-50	0.28
Pyrite	FeS_2	4654	314	67.5	23.39
Hematite	Fe_2O_3	5245	2622-19931	500-3800	0.27
Monazite	$(La,Ce)PO_4$	5100	55.59	10.9	0
Chlorite	$(Mg_3,Fe_2)Al(AlSi_3)O_{10}(OH)_8$	3000	4673	1558	0.6
Biotite	$K(Mg,Fe)_3[Si_3AlO_{10}](OH,F)_2$	3020-3120	96-150	32-48	0.37
Titanite	$CaTiSiO_5$	3480	(-)	(-)	0.29
Hornblende	(2.1% Fe)	2900-3500	9000	2500-3000	0.02

Table. 5: The mineralogy (%wt) per fraction of copper ore B (0.25-0.5 mm) obtained by MLA

	Data Source	**Copper ore B 0.25-0.50 mm 0-30**	**Copper ore B 0.25-0.50 mm 30-100**	**Copper ore B 0.25-0.50 mm 100-185**
	Mineral	**Mineral Weight (%)**	**Mineral Weight (%)**	**Mineral Weight (%)**
Rel_magnetic	**Chalcopyrite**	1.91	1.23	0.66
	Bornite	1.66	1.26	0.46
	Covellite	0.00	0.00	0.00
	Chalcocite	7.81	6.30	2.16
	Sphalerite	0.17	0.14	0.03
	Galena	0.00	0.00	0.00
	Rutile	0.02	0.07	0.09

	Pyrite	60.88	46.29	5.39
	Hematite	1.20	5.60	0.11
	Chlorite	0.07	0.11	0.00
	Biotite	0.54	0.50	0.30
	Titanite	0.03	0.03	0.06
	Hornblende	0.25	0.10	0.07
Total Rel_magnetic		74.54	61.63	9.33
Rel_diamagnetic	**Quartz**	10.21	18.02	52.41
	Illite	8.89	12.88	24.95
	Others	6.36	7.47	13.31
Total Rel_diamagnetic		25.46	38.37	90.67

Table.6: The mineralogy (%wt) per fraction of copper ore B (2-3 mm) obtained by MLA

	Data Source	**Copper ore B 2-3 mm 0-30**	**Copper ore B 2-3 mm 30-100**	**Copper ore B 2-3 mm 100-185**
	Mineral	**Mineral Weight (%)**	**Mineral Weight (%)**	**Mineral Weight (%)**
Rel_magnetic	**Chalcopyrite**	0.48	0.00	0.53
	Bornite	1.09	0.00	0.18
	Covellite	0.00	0.00	0.00
	Chalcocite	5.58	0.00	0.69
	Sphalerite	0.13	0.00	0.01
	Galena	0.00	0.00	0.00
	Rutile	0.01	0.00	0.02
	Pyrite	73.31	0.00	2.94
	Hematite	6.22	0.00	0.01
	Chlorite	1.83	0.00	0.00
	Biotite	0.12	0.00	1.28
	Titanite	0.97	0.00	0.03
	Hornblende	0.05	0.00	0.02
Total Rel_magnetic		89.79	0.00	5.73
Rel_diamagnetic	**Quartz**	2.72	0.00	34.52
	Illite	4.66	0.00	38.62
	Others	2.83	0.00	21.13
Total Rel_diamagnetic		10.21	0.00	94.27

Table. 7: The mineralogy (%wt) per fraction of nickel ore (0.25-0.5 mm) obtained by MLA

	Data Source	Nickel ore 0.25-0.50 mm 0-30	Nickel ore 0.25-0.50 mm 30-100	Nickel ore 0.25-0.50 mm 100-185
	Mineral	**Mineral Weight (%)**	**Mineral Weight (%)**	**Mineral Weight (%)**
Rel_magnetic	**Pentlandite**	17.24	13.76	0.00
	Pyrrhotite	26.33	2.78	0.00
	Pyrite	5.18	6.14	0.00
	Chalcopyrite	0.97	1.00	0.00
	Ilmenite	0.19	0.24	0.00
	Magnetite	4.34	0.86	0.00
	Chromite	2.07	0.33	0.00
	Titanite	0.03	0.16	0.00
	Hornblende	15.19	24.54	0.00
	Chlorite	5.55	7.43	0.00
	Biotite	3.37	4.84	0.00
Total Rel_magnetic		80.46	62.07	0.00
Rel_diamagnetic	**Talc**	8.74	15.12	0.00
	Dolomite	2.90	5.35	0.00
	Calcite	0.91	3.12	0.00
	Quartz	1.72	4.42	0.00
	Others	5.28	9.92	0.00
Total Rel_diamagnetic		19.54	37.93	0.00

Table. 8: The mineralogy (%wt) per fraction of nickel ore (2-3 mm) obtained by MLA

	Data Source	Nickel ore 2-3 mm 0-30	Nickel ore 2-3 mm 30-100	Nickel ore 2-3 mm 100-185
	Mineral	**Mineral Weight (%)**	**Mineral Weight (%)**	**Mineral Weight (%)**
Rel_magnetic	**Pentlandite**	8.54	0.00	0.00
	Pyrrhotite	18.50	0.00	0.00
	Pyrite	3.70	0.00	0.00
	Chalcopyrite	0.96	0.00	0.00
	Ilmenite	0.13	0.00	0.00
	Magnetite	2.70	0.00	0.00
	Chromite	1.05	0.00	0.00
	Titanite	0.08	0.00	0.00
	Hornblende	26.24	0.00	0.00
	Chlorite	8.07	0.00	0.00
	Biotite	3.75	0.00	0.00
Total Rel_magnetic		73.72	0.00	0.00
Rel_diamagnetic	**Talc**	10.16	0.00	0.00
	Dolomite	4.33	0.00	0.00
	Calcite	1.44	0.00	0.00
	Quartz	1.23	0.00	0.00
	Others	9.12	0.00	0.00
Total Rel_diamagnetic		26.28	0.00	0.00

Table. 9: The mineralogy (%wt) per fraction of copper ore A (0.25-0.5 mm) obtained by MLA

	Data Source	Copper ore A 0.25-0.50 mm 0-30	Copper ore A 0.25-0.50 mm 30-100	Copper ore A 0.25-0.50 mm 100-185
	Mineral	**Mineral Weight (%)**	**Mineral Weight (%)**	**Mineral Weight (%)**
Rel_magnetic	**Magnetite**	36.29	0.73	0.04
	Chalcocite	0.00	0.00	0.00
	Chalcopyrite	1.45	0.81	0.22
	Uranothorianite	0.37	0.11	0.00
	Galena	0.00	0.00	0.00
	Bornite	0.87	0.58	0.10
	MA_Spinel	0.25	0.04	0.08
	Valleriite	0.31	0.30	0.03
	Chlorite_group	1.21	1.01	0.26
	Biotite	12.66	1.10	3.19
	Monazite	0.07	0.04	0.04
	Baddeleyite	0.06	0.06	0.03
	Serpentine_ group	0.14	0.44	0.20
	Olivine	7.91	9.48	2.11
Total Rel_magnetic		61.60	14.71	6.31
Rel_ diamagnetic	**Dolomite**	6.98	17.25	12.79
	Apatite	7.07	13.11	13.75
	Calcite	24.16	54.88	67.14
	Others	0.19	0.05	0.02
Total Rel_diamagnetic		38.40	85.29	93.69

Table. 10: The mineralogy (%wt) per fraction of copper ore A (2-3 mm) obtained by MLA

	Data Source	Copper ore A 2-3 mm 0-30	Copper ore A 2-3 mm 30-100	Copper ore A 2-3 mm 100-180
	Mineral	**Mineral Weight (%)**	**Mineral Weight (%)**	**Mineral Weight (%)**
Rel_magnetic	**Magnetite**	40.02	0.00	0.00
	Chalcocite	0.00	0.00	0.00
	Chalcopyrite	0.60	0.00	0.00
	Uranothorianite	0.07	0.00	0.00
	Galena	0.00	0.00	0.00
	Bornite	0.31	0.00	0.00
	MA_Spinel	0.32	0.00	0.00

	Valleriite	0.24	0.00	0.00
	Chlorite_group	0.29	0.00	0.00
	Biotite	9.94	0.00	0.00
	Monazite	0.06	0.00	0.00
	Baddeleyite	0.02	0.00	0.00
	Serpentine_ group	0.27	0.00	0.00
	Olivine	2.98	0.00	0.00
Total Rel_magnetic		55.12	0.00	0.00
Rel_diamagnetic	**Dolomite**	7.76	0.00	0.00
	Apatite	3.23	0.00	0.00
	Calcite	33.70	0.00	0.00
	Others	0.19	0.00	0.00
Total Rel_diamagnetic		44.88	0.00	0.00